Structure
Article

# Allosteric Mechanism Controls Traffic in the Chaperone/Usher Pathway

Xiao Di Yu,[1,4,5] Anatoly Dubnovitsky,[1,4] Alex F. Pudney,[3] Sheila MacIntyre,[3] Stefan D. Knight,[1,*] and Anton V. Zavialov[1,2,*]
[1]Department of Molecular Biology, Uppsala BioCenter, Swedish University of Agricultural Sciences, BMC, Box 590, SE-753 24 Uppsala, Sweden
[2]Department of Chemistry, University of Turku, Turku, JBL, BioCity 6A, FIN-20520 Turku, Finland
[3]School of Biological Sciences, Animal and Microbial Sciences Building, University of Reading, Reading RG6 6AJ, UK
[4]These authors contributed equally to this work
[5]Present address: The F. M. Kirby Neurobiology Center, Boston Children's Hospital, Department of Neurology, Harvard Medical School, Boston, MA 02115, USA
*Correspondence: stefan.knight@molbio.slu.se (S.D.K.), anton.zavialov@molbio.slu.se (A.V.Z.)
http://dx.doi.org/10.1016/j.str.2012.08.016

## SUMMARY

**Many virulence organelles of Gram-negative bacterial pathogens are assembled via the chaperone/usher pathway. The chaperone transports organelle subunits across the periplasm to the outer membrane usher, where they are released and incorporated into growing fibers. Here, we elucidate the mechanism of the usher-targeting step in assembly of the *Yersinia pestis* F1 capsule at the atomic level. The usher interacts almost exclusively with the chaperone in the chaperone:subunit complex. In free chaperone, a pair of conserved proline residues at the beginning of the subunit-binding loop form a "proline lock" that occludes the usher-binding surface and blocks usher binding. Binding of the subunit to the chaperone rotates the proline lock away from the usher-binding surface, allowing the chaperone-subunit complex to bind to the usher. We show that the proline lock exists in other chaperone/usher systems and represents a general allosteric mechanism for selective targeting of chaperone:subunit complexes to the usher and for release and recycling of the free chaperone.**

## INTRODUCTION

Many biological functions depend on the precise assembly of larger complex structures from smaller protein subunits. This requires accurate control over each biogenesis step from synthesis of subunits to targeting, often membrane translocation, and finally assembly of the supramolecular structure. The assembly of fibrillar adhesive surface organelles from pilin subunits via the chaperone/usher (CU) pathway in Gram-negative bacteria represents one of the best studied examples of a biological assembly process (Waksman and Hultgren, 2009; Zav'yalov et al., 2010; Zavialov et al., 2007) (Figure 1). These organelles consist of linear fibers of noncovalently linked immunoglobulin (Ig)-like modules (Sauer et al., 2002; Zavialov et al., 2003b). The Ig-like modules are made by combining two protein subunit chains. The first six strands of the Ig-like fold, the bulk of the module, all come from a single chain. The seventh (G) strand is provided in trans by the N-terminal "donor strand" region of the preceding subunit in the fiber. Since this region substitutes for the G strand that is present at the C terminus of Ig domains, but missing in pilin subunits, thereby completing the Ig-like fold of the module, this type of interaction was termed donor strand complementation (Choudhury et al., 1999; Sauer et al., 1999).

Depending on the subunit type(s) and composition, the fibers coil into structures of different architecture. The number of different subunit types assembled and the complexity of surface organelle morphology inversely correlate with the length of subunit-binding motifs in chaperones (Zav'yalov et al., 2010). This enables the classification of CU machineries and corresponding organelles into FGS and FGL systems (Hung et al., 1996; Zav'yalov et al., 1995; Zavialov et al., 2007). *Escherichia coli* Pap and Type-1 (Fim) CU systems have been used as prototypes of the FGS family, while the *Yersinia pestis* Caf CU system is the best-studied FGL system (Zavialov et al., 2007). The Caf CU pathway (Caf1M/Caf1A) assembles F1 fibers that consist of only one type of subunit (Caf1). The thin and flexible F1 fibers tend to curl up and agglomerate into a dense amorphous structure with the appearance of a capsule (F1 capsular antigen).

In isolation, fimbrial subunits have poor stability and in vivo either aggregate or are rapidly degraded (Chapman et al., 1999; MacIntyre et al., 2001). The periplasmic chaperones bind fimbrial subunits as they enter the periplasm, thereby promoting their rapid folding and stabilizing them in a high-energy, assembly competent conformation (Sauer et al., 2002; Yu et al., 2012; Zavialov et al., 2003b, 2005). They do so by providing a folding platform consisting of the $A_1$ and $G_1$ strands of the first Ig-like domain of the chaperone, with the $G_1$ ("donor") strand acting as a "stand-in," completing the Ig fold of the subunit (Yu et al., 2012).

Subunit assembly takes place at the usher and occurs via a donor strand exchange (DSE) mechanism, in which the chaperone capping the subunit at the base of a growing fiber is displaced by the N-terminal donor strand of an incoming subunit. The usher consists of four soluble periplasmic domains and a transmembrane β-barrel that forms a channel for secretion of the fiber (Dubnovitsky et al., 2010; Nishiyama et al., 2005; Phan et al., 2011; Remaut et al., 2008; Yu et al., 2009) (Figure 1).

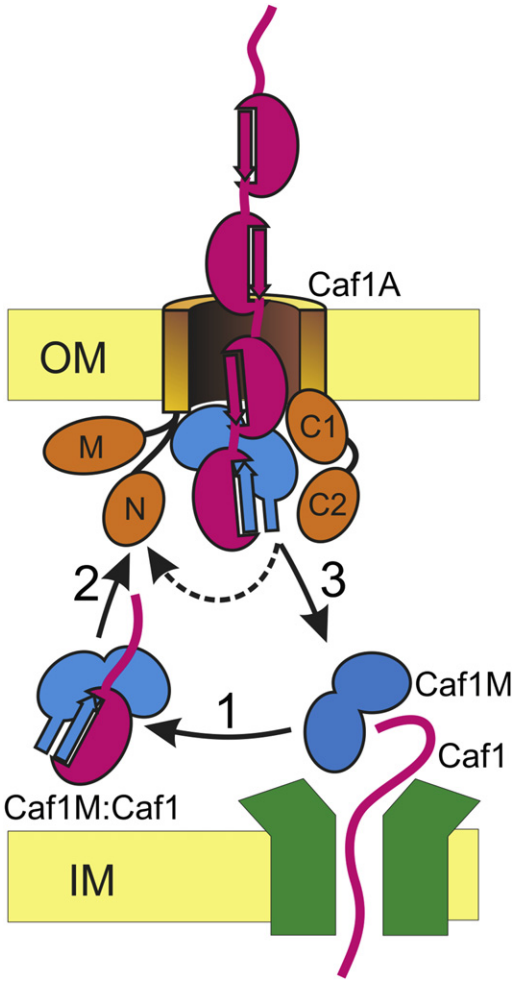


**Figure 1. Schematic Illustration of F1 Fiber Assembly**
Major steps: (1) Formation of the Caf1M:Caf1 complex; (2) binding to activated Caf1A; (3) fiber elongation and release of Caf1M. N, usher N-terminal domain; M, usher middle domain; C1 and C2, usher C-terminal domains. The mechanism of selective binding of Caf1-bound Caf1M to N and C-terminal domains is not clear. Hypothetical interaction of Caf1-free Caf1M with Caf1A is indicated by a dashed line. See also Figure S1.

Two of the periplasmic usher domains, the N-terminal domain (UND) and the middle domain, are involved in initial binding of chaperone:subunit complexes and "plugging" the translocation pore, respectively. The plug domain of the Caf1A usher shows structural similarity to the Caf1 subunit (Yu et al., 2009). Two tandem Ig-like C-terminal domains (UCD1 and UCD2) (Dubnovitsky et al., 2010; Phan et al., 2011; Remaut et al., 2008) bind to the chaperone capping the base of a growing fiber. Recent structural characterization of assembly complexes in the type 1 system led to the following general model for assembly (Phan et al., 2011). In FGS systems, such as P or type-1 fimbriae, the complex of the two-domain adhesin subunit with chaperone must be added first to the UCDs to trigger release of the plug domain and open the channel. The next and following chaperone:subunit preassembly complexes bind to the UND, which is tethered to the N-terminus of the barrel domain by a relatively long flexible linker. Modeling (Phan et al., 2011) suggests that the free UND would be able to capture a new preassembly complex from the periplasmic pool and position it with its free N-terminal donor strand in close proximity to the P5 DSE initiation site (Remaut et al., 2006) of the acceptor cleft of the UCD-bound subunit, aligning the system for DSE. Addition of the new subunit to the base of the fiber through DSE is thought to be accompanied by release of the chaperone from the acceptor subunit, transfer of the attacking complex from the UND to the UCDs, and translocation of one subunit through the usher pore. The detailed mechanism of this process, in particular, the specificity of binding and release, is not yet understood.

The usher must be able to distinguish the preassembly complex from free chaperone or free chaperone would compete for and inhibit assembly (Figure 1). Indeed, chaperone-subunit complexes were found to bind to the usher, whereas no binding of free chaperone to the usher was detected in vitro (Dodson et al., 1993; Saulino et al., 1998). Structural studies on the classical FGS CU Fim system for assembly of type-1 fimbriae suggested a possible basis for such discrimination (Nishiyama et al., 2005). The crystal structure of the N-terminal domain of the FimD usher ($FimD_N$) bound to the complex of the FimC chaperone and pilin domain of subunit FimH revealed that the usher-chaperone contact contributes most of the interactive binding area, while the contact between the usher and subunit is small. Nevertheless, it was proposed that usher-subunit contacts might contribute sufficient binding energy to ensure the selective recognition of the complex. However, a more recent structure of the $FimD_N$:FimC:FimF complex from the same system revealed a significantly smaller interactive area between the usher and subunit (Eidam et al., 2008), weakening this hypothesis.

Here, we investigate the basis for discrimination between the free chaperone and preassembly complex in the Caf CU system. We determined the X-ray structure for the monomeric Caf1M chaperone, the N-terminal domain of the Caf1A usher, and the Caf1M:Caf1 preassembly complex bound to this domain. By comparison of these and previously obtained structures, together with protein engineering and binding studies, we show that the affinity between chaperone and usher is allosterically regulated by the subunit through a mechanism that is most likely conserved and commonly used in CU systems.

## RESULTS AND DISCUSSION

### Preassembly Complex Binding Domain in Caf1A

We began our study with identification of Caf1M:Caf1-binding segments in Caf1A. Based on the sequence homology between Caf1A and FimD, we introduced deletions in the N-terminal region of the mature sequence of Caf1A. The deletion of residues 12–27 and 12–40 did not significantly affect Caf1A insertion into the outer membrane (Figure S1A available online). However, they completely abolished F1 capsule formation (Figure S1B) and resulted in accumulation of Caf1M:Caf1 complexes in the periplasm (Figure S1C). These results indicate that Caf1A binds chaperone:subunit complexes via a domain located at the N-terminus of the protein, as does FimD. Indeed, overexpression of an N-terminal fragment (residues 1–158, including signal sequence) of the Caf1A precursor in *E. coli* resulted in high-level accumulation of a soluble protein in the periplasm. The isolated

**Table 1. Data Collection and Refinement Statistics**

| | $Caf1A_N$ | $Caf1A_N$:Caf1M: Caf1 complex | Caf1M-Δ2-12, -Δ113-129 | Caf1M-Y40A:Caf1 | Caf1M-A114-insKDKDTN:Caf1 |
|---|---|---|---|---|---|
| Data collection | | | | | |
| Resolution (Å) | 30.0–2.00 | 30.0–1.8 | 62.0–1.45 | 68.0–2.07 | 48.0–2.65 |
| Space group | $C222_1$ | $P2_1$ | $P6_5$ | $P2_1$ | $P2_1$ |
| Unit cell parameters (Å) | 61.9 × 68.6 × 192.2 | 35.3 × 77.4 × 95.9 β = 98.5° | 56.7 × 56.7 × 248.2 | 35.1 × 68.9 × 65.0 β = 94.17° | 35.5 × 69.3 × 66.0 β = 94.82° |
| Unique reflections | 27,484 | 47,312 | 79,538 | 18,931 | 9,383 |
| $<I/\sigma(I)>$ | 16.0 (3.0) 2.07–2.00 | 17.5 (2.5) 1.90–1.80 | 5.80 (2.0) 1.53–1.45 | 8.27 (2.0) 2.18–2.07 | 6.3 (2.0) 2.79–2.66 |
| Multiplicity | 4.9 (2.2) | 3.4 (2.6) | 8.52 (7.5) | 3.63 (3.7) | 3.7 (3.7) |
| Completeness (%) | 97.0 (87.0) | 96.9 (81.5) | 99.7 (99.2) | 99.8 (99.9) | 99.9 (99.9) |
| $R_{merge}$ (%) | 8.0 (32.0) | 6.0 (32.0) | 6.0 (39.0) | 7.0 (35.0) | 11.0 (37.0) |
| Refinement | | | | | |
| Resolution (Å) | 30.0–2.0 | 30.0–1.8 | 28.8–1.5 | 47.3–2.1 | 29.7–2.7 |
| Number of reflections (working + test set) | 25,948 + 1,365 | 43,506 + 2,310 | 65,474 + 3,446 | 17,957 + 975 | 8906 + 446 |
| $R_{work}$ | 20.5 | 18.3 | 16.6 | 19.2 | 22.1 |
| $R_{free}$ | 26.1 | 23.7 | 18.8 | 24.8 | 25.1 |
| Average B-factor ($Å^2$) | 37.6 | 33.8 | 15.8 | 25.5 | 21.7 |
| rmsd stereochemistry | | | | | |
| Bonds (Å) | 0.016 | 0.022 | 0.006 | 0.007 | 0.006 |
| Angles (°) | 1.594 | 1.758 | 1.126 | 1.080 | 1.441 |
| Coordinate error (Å) | 0.14 | 0.09 | 0.13 | 0.27 | 0.31 |
| Ramachandran plot | | | | | |
| Residues in the core regions (%) | 99.2 | 99.0 | 98.40 | 98.59 | 98.29 |
| Residues in additional allowed regions (%) | 0.8 | 1 | 1.60 | 1.41 | 1.71 |
| Number of molecules in asymmetric unite | 4 | 1 | 2 | 1 | 1 |

Values for high-resolution shells are shown in parenthesis. The limits of high resolution shells are indicated. See also Figure S5.

domain was capable of autonomous folding and showed high thermodynamic stability (Figure S1D). To highlight the N-terminal localization of the domain, we have denoted it $Caf1A_N$.

$Caf1A_N$ was purified from periplasmic extracts and crystallized, and its 2 Å crystal structure was solved (Figure S1E; Table 1). The asymmetric unit contains four $Caf1A_N$ molecules with very similar structures. None of the molecules have electron density for the N- and C-terminal parts of $Caf1A_N$ before Asp18 and after Phe124, respectively, suggesting that these sequences are not structured in $Caf1A_N$. The core structure of the domain is made of a small five-stranded pseudobarrel sealed at the top and bottom with connective loops and helices α1 (bottom) and α2 (top) (Figure S1E). This structure is similar to that of the N-terminal domain of the FimD usher (Nishiyama et al., 2005). Superpositioning of these domains aligns 88 Cα atoms with a root-mean-square deviation (rmsd) value of 1.3 Å (Figures S1E and S1F). The high degree of structural similarity between N-terminal domains of Caf1A and FimD ushers, representing ushers from the FGL and FGS CU pathways, respectively, suggests that the mechanism of chaperone:subunit complex binding by ushers is highly conserved and is likely to be similar in all CU systems.

## $Caf1A_N$ Binds to Caf1-Loaded, but Not Free Caf1M

To quantitatively characterize binding between $Caf1A_N$ and Caf1M:Caf1, surface plasmon resonance (SPR) was used. $Caf1A_N$ was covalently immobilized to a sensor chip, and the binding of the Caf1M:Caf1 complex was measured by recording the SPR signal after addition of the complex in the liquid phase. As binding was too dynamic to follow accurately in real time, we analyzed the reaction only at equilibrium (Figure S1G), allowing accurate estimation of the dissociation constant (2.42 ± 0.24 μM; Table 2). The value obtained is similar to that previously determined for binding of $FimD_N$ to FimC loaded with tip fibrillum subunits FimH or FimF and higher than that of $FimD_N$ binding to FimC loaded with the pilus rod subunit, FimA (Nishiyama and Glockshuber, 2010; Nishiyama et al., 2003).

No binding between $Caf1A_N$ and free Caf1M was detected in similar experiments at concentrations of Caf1M as high as 400 μM (Table 2). Binding of Caf1M:Caf1 to $Caf1A_N$ was not inhibited by Caf1M, even at a 500-fold excess of Caf1M over the Caf1M:Caf1 complex (Figure S2). Thus Caf1A is able to specifically recognize Caf1-loaded Caf1M and selectively bind to it, even at high excess of free Caf1M.

**Table 2. Effect of Mutations on the Binding of Caf1M:Caf1 and Caf1M to Caf1A$_N$**

| Mutation | *Kd* ($\mu M^{-1}$) |
|---|---|
| Caf1A$_N$–(Caf1M:Caf1) | |
| Wild-type | 2.42 ± 0.24 |
| Caf1-A141G | 4.0 ± 2.1 |
| Caf1M-P104A | 61.4 ± 3.5 |
| Caf1M-P104S | 70.1 ± 1.3 |
| Caf1M-P103SP104A | >80 |
| Caf1M-Y12G | 7.0 ± 4.4 |
| Caf1M-Y40A[a] | 39.4 ± 10 |
| Caf1M Y40AY12G | >100 |
| Caf1M-L43A | 60.7 ± 1.6 |
| Caf1M-Ins114KDKDTN[a] | 4.7 ± 0.4 |
| Caf1A$_N$-F4A | ND[b] |
| Caf1A$_N$-M8A | 5.0 |
| Caf1A$_N$-T7GM8A | 5.1 |
| Caf1A$_N$-Caf1M | |
| Wild-type | ND[b] |
| Caf1M-Δ113-129 | >450 |
| Caf1M-Δ2-12 | >260 |
| Caf1M-Δ2-12, Δ113-129[a] | >240 |
| Caf1M-Δ106-111 | 111 ± 40.3 |
| Caf1M-Δ106-113 | 29.5 ± 8.7 |
| Caf1M-Δ106-123 | 33.8 ± 3.6 |
| Caf1M-Δ106-125 | 28.0 ± 2.9 |
| Caf1M-Δ106-127 | 17.0 ± 2.3 |
| Caf1M-Δ106-129 | 9.8 ± 1.0 |

The data for the entire list of mutants can be found in Tables S1 and S2; see also Figure S2.
[a]Structure available, this study.
[b]Not detected.

## Caf1A-Caf1 Contact Is Not Essential for Caf1M:Caf1 Recognition by Caf1A

To elucidate how Caf1A selectively recognizes the Caf1M:Caf1 complex, we determined a crystal structure of the Caf1A$_N$:Caf1M:Caf1 complex. The structure of Caf1A$_N$:Caf1M:Caf1 was solved by molecular replacement using the crystal structure of Caf1M:Caf1 and refined at 1.8 Å resolution to R = 18.3% and $R_{free}$ = 23.7% (Table 1; Figure 2A). To facilitate the following discussion, we have labeled residue numbers for Caf1A and Caf1M in the complex with "a" and "m" superscripts, respectively.

The structures of Caf1M:Caf1 and the core of Caf1A$_N$ remain essentially unchanged after binding. The largest conformational change occurs in the N-terminal 1-17 amino acid sequence of Caf1A$_N$, which becomes ordered in Caf1A$_N$:Caf1M:Caf1 (Figure 2A; Figure S1E). This sequence, together with the following helix α1 makes up the largest part of the domain's binding surface (626 Å$^2$, ~60%) (Figure 2B). Nine residues in these segments (Tyr2[a], Thr3[a], Phe4[a], Thr7[a], Met8[a], Leu9[a], Leu17[a], Val19[a], and Phe22[a]) establish van der Waals interactions with seven closely situated residues in Caf1M, including four hydrophobic residues exposed on the surface of the DCFG β sheet

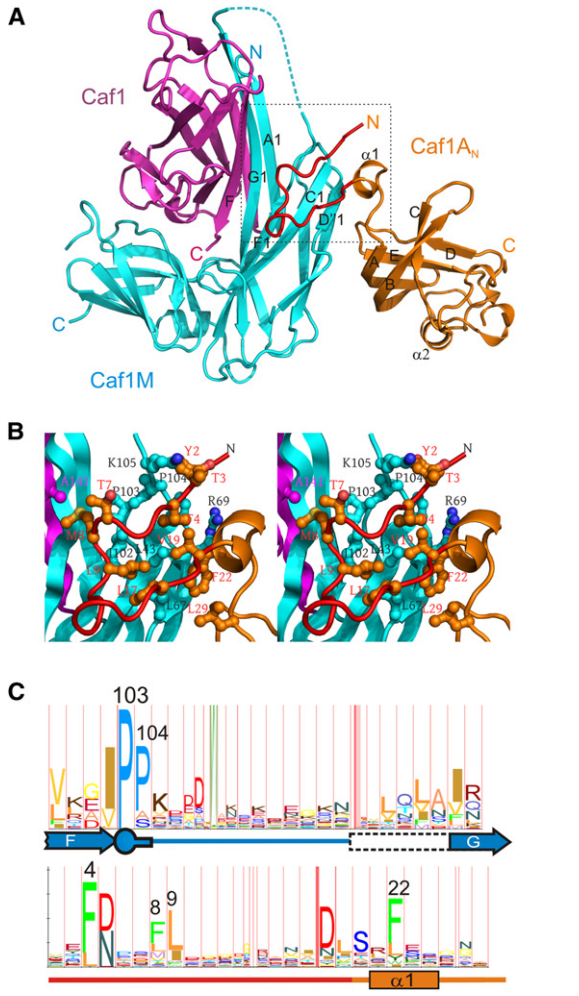


**Figure 2. Caf1A$_N$-Caf1M Contact Dominates the Binding Interface between Caf1A$_N$ and Caf1M:Caf1**

(A) Crystal structure of the Caf1A$_N$:Caf1M:Caf1 complex (cartoon diagrams). The N-terminal region of Caf1A$_N$ that becomes structured upon binding is shown in red; the rest of Caf1A$_N$ is shown in orange. Caf1M and Caf1 are shown in cyan and magenta, respectively. The disordered part of the $F_1G_1$ loop in Caf1M (not observed in crystal structures) is indicated with a dashed line. The β strands in Caf1M and Caf1, carrying usher-binding residues, as well as all secondary structure elements in Caf1A$_N$ are labeled. The square indicates the fragment of the structure shown in (B).

(B) The binding interface between Caf1A$_N$ and Caf1M:Caf1 (cartoon diagram, stereo view). The color-coding is the same as in (A). The interactive residues are shown as balls-and-sticks and labeled. The carbon atoms are shown in the color of the chain; oxygen and nitrogen atoms are shown in red and blue, respectively.

(C) Caf1A$_N$-Caf1M-binding contact involves highly conserved residues. Graphical representations (sequence logos) of chaperone $F_1$-$G_1$ (above) and usher N-terminal (below) regions in multiple sequence alignment of periplasmic chaperones and usher proteins, PF00345 and pfam00577, respectively. Sequence logos were generated using the WEBLOGO program at http://weblogo.berkeley.edu/logo.cgi. The most highly conserved positions are labeled according to Caf1M and Caf1A sequences (Pro103[m] and Pro104[m] in Caf1M and Phe4[a] in Caf1A are the most conserved). Secondary structure representations are shown below the diagrams. Pro103[m] and Pro104[m] are indicated by a keyhole symbol. The part of the $G_1$ strand that becomes ordered upon Caf1 binding is indicated by an arrow with a dashed outline.

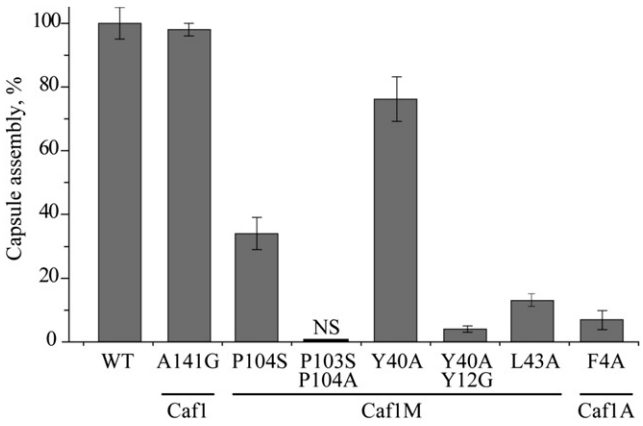


**Figure 3. Effects of Replacements of Residues Involved in Caf1A$_N$-(Caf1M:Caf1) Binding or Its Regulation on F1 Capsule Assembly**

Surface exposed Caf1 was quantitated in a surface immunofluorescence assay. The fluorescence signal of cells carrying the wild-type *Caf* operon (145971) was treated as 100% efficiency of capsule assembly. Error bars indicate standard deviation (n = 3). NS, no signal above background.

of domain 1 (Pro41$^m$, Leu43$^m$, Leu67$^m$, and Ile102$^m$), Pro103$^m$ and Pro104$^m$ at the beginning of the $F_1G_1$ loop, and the aliphatic part of the side chain of Arg69$^m$. Together, these residues form a hydrophobic usher-binding surface (UBS). All the interface residues are highly conserved, in particular, Pro103$^m$ (invariant), Pro104$^m$, and Phe4$^a$ (Figure 2C). In addition, there are a number of residues contributing Caf1A-Caf1M contacts, which are not arranged in binding clusters.

Caf1 contributes only ~3% (36 Å$^2$) to the usher-binding area of the preassembly complex (~1,069 Å$^2$), largely attributed to Ala141. The side chain of Met8$^a$ and atom Cδ2 of Thr7$^a$ are located within 3.9–4.4 Å from the Cα and Cβ atoms of Ala141 in Caf1, thus providing weak van der Waals interactions. In addition, a weak interaction is formed between the Cε atom of Met8$^a$ and the C atom of Val142 of Caf1. Such a small Caf1A$_N$-Caf1 interactive area is surprising in view of the hypothesis proposed by Nishiyama and coauthors (Nishiyama et al., 2005) that contacts between the usher and the subunit are responsible for the selective recognition of preassembly complexes. How could such a small interface influence the binding specificity?

Changing Ala141 to Gly (essentially halving the interactive area) had no effect on Caf1M:Caf1 binding to Caf1A$_N$ (Table 2) and F1 assembly (Figure 3). Similarly, mutation of Met8$^a$ to Ala did not significantly affect binding. In contrast, substitutions of Leu43$^m$ or Phe4$^a$ to Ala residues, decreasing the Caf1A-Caf1M interactive area by 7.4% and 11.6%, respectively, dramatically reduced both the affinity between Caf1A$_N$ and the Caf1M:Caf1 preassembly complex and the efficiency of F1 capsule assembly.

In conclusion, both the structural and functional studies clearly demonstrate that the Caf1A-Caf1 contact is not important for binding of Caf1M:Caf1 to Caf1A$_N$, and it cannot serve as the main determinant for selective recognition of the subunit-loaded chaperone by the usher. So, which mechanism is responsible for this?

## Role of Caf1M Tetramerization in the Selective Binding of Caf1-Loaded Caf1M by Caf1A

Caf1M equilibrates between the active monomeric and inactive tetrameric forms (Zavialov and Knight, 2007). Caf1M tetramerization might inhibit Caf1A-Caf1M binding and favor binding between Caf1A and Caf1M:Caf1 by reducing the concentration of free Caf1M. To study the possible contribution of this effect on Caf1M:Caf1 targeting to Caf1A, we probed the binding between Caf1A and Caf1M, carrying a deletion of residues 2–12 at the N-terminus and/or 113–129 in the $F_1G_1$ loop. The deleted sequences are apparently not involved in Caf1A binding, but their deletion completely abolishes Caf1M tetramerization, resulting in accumulation of monomers (Zavialov and Knight, 2007).

In contrast to wild-type Caf1M, these mutants bound to Caf1A$_N$ at high concentrations (Table 2). However, binding was not saturated, suggesting an apparent dissociation constant of more than 260 μM, at least 100 times higher than the dissociation constant for binding of Caf1A$_N$ to Caf1M:Caf1 (Table 2). Indeed, these mutants inhibited the Caf1A$_N$-(Caf1M:Caf1) binding to only ~40% at 500-fold excess over the Caf1M:Caf1 complex (Figure S2). Hence, Caf1M tetramerization is unlikely to represent a decisive controlling mechanism. The finding of such a low affinity of monomeric Caf1M to Caf1A$_N$ suggests that regulation may depend on conformational differences between free and loaded Caf1M.

## Caf1M Binding to Caf1A Is Allosterically Controlled by Caf1

To investigate the hypothesis that monomeric Caf1M takes on a conformation that prevents it from efficiently binding to Caf1A$_N$, we determined the 1.5 Å crystal structure of the Caf1M-Δ2-12, Δ113-129 mutant.

The asymmetric unit contained two Caf1M monomers (Figure S3). They had nearly identical structures, except for small differences in some loops, most likely caused by crystallographic contacts. Importantly, the UBS and its surroundings were not affected by crystallographic contacts. The structure had almost no electron density for residue 13 and poor density for residue 14 at the N-terminus and no electron density for the sequence from residue 105 to 134 in the $F_1G_1$ hairpin. This supports partial proteolysis data for diluted (monomeric) wild-type Caf1M (Chapman et al., 1999) that suggests that sequences up to residue 14 and between residues 105 and 134 are unstructured in the Caf1M monomer.

Structural comparison of free and Caf1-bound Caf1M revealed significant conformational differences, in particular, in the N-terminal domain (Figure 4A). In Caf1-bound Caf1M, residues 8–13 and 125–133 form the $A_1$ and $G_1$ Caf1-binding strands. In total, Caf1 binding causes structuring of about 10% of the residues in domain 1 of Caf1M. Not surprisingly, this change distorts the DCFG β sheet in this domain. The extended $G_1$ donor strand, which is firmly docked in the subunit acceptor cleft, forms additional hydrogen bonds to the end of the $F_1$ strand, pulling its end closer to the $G_1$ strand and simultaneously causing the $F_1$ strand to twist, affecting positions of several residues, including the UBS residue Ile102$^m$ (Figures 4A and 4B). However, the most striking difference is observed in the positions of Pro103$^m$ and Pro104$^m$ at the beginning of the $F_1G_1$ loop (Figure 4B). In free Caf1M, Pro104$^m$ occupies a hydrophobic

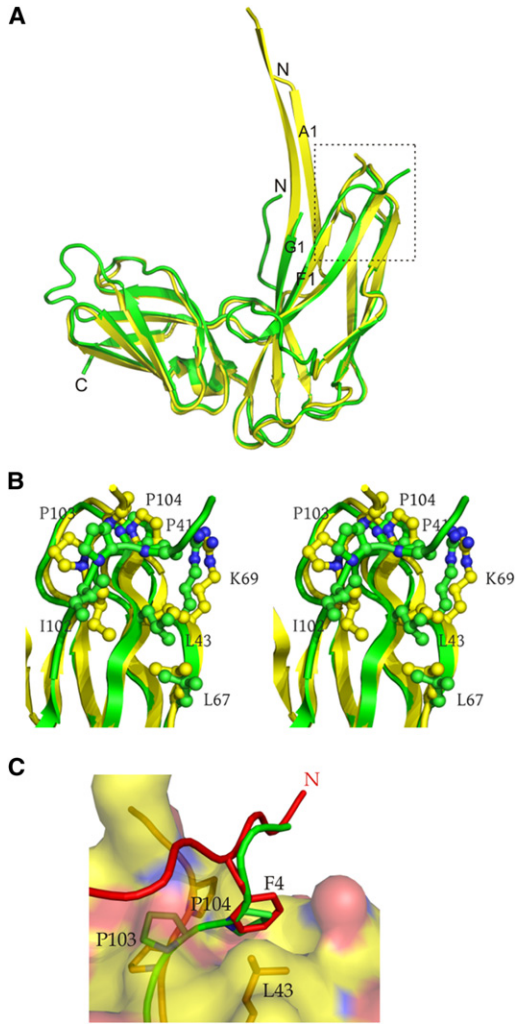


**Figure 4. Pro-Pro Lock Occludes the Usher-Binding Surface in Free Caf1M**

(A) Superposition of free Caf1M (green) and Caf1M from the Caf1M:Caf1 complex (yellow). $A_1$, $F_1$, and $G_1$ strands and N and C termini are labeled. The square indicates the fragment of the structure shown in (B).

(B) Superposition of the Caf1A binding site in Caf1-free (green) and Caf1-bound (yellow) Caf1M (stereo view).

(C) The Pro-Pro lock prevents binding of Phe4[a] to the UBS. Structures of the Caf1M monomer and $Caf1A_N$:Caf1M:Caf1 complex are superimposed. The Pro-Pro lock fragment of Caf1M monomer is shown in green; $Caf1A_N$ and Caf1M in the complex are shown in red and yellow, respectively. The molecular surface of Caf1M in the complex is also shown.

See also Figure S3.

pocket between the side chains of Pro41[m], Leu43[m], and Ile102[m] and the aliphatic part of the side chain of Arg69[m], which all belong to the UBS. Hence, in free Caf1M, the UBS is in a closed or collapsed conformation that prevents binding to the usher (Figures 4B and 5A). In contrast, in Caf1-bound Caf1M, Pro103[m] and Pro104[m] are rotated to move Pro104[m] out of the UBS. We will refer to this second conformation as an open UBS (Figures 4B and 5B).

In the closed UBS, the distance between Cα atoms of Pro104[m] and Leu43[m] is about 2.5 Å shorter than that in the open UBS (Table S3). Not surprisingly, structural comparison of free Caf1M and $Caf1A_N$:Caf1M:Caf1 revealed that the closed UBS conformation cannot form optimal interactions with the binding residues of $Caf1A_N$. Most strikingly, Phe4[a], which is essential for binding (Table 2; Figure 3), cannot insert into its local binding pocket, because in the closed UBS conformation, this is occupied by Pro104[m] (Figure 4C).

Caf1M has the same open UBS conformation in the preassembly complex and the complex bound to the usher. This is reflected in similar values for the distances between Cα atoms of Pro104[m] and Leu43[m] (8.1–8.3 Å) in all structures determined so far that include Caf1M:Caf1 (Caf1M:Caf1, Caf1M:Caf1:Caf1, and $Caf1A_N$:Caf1M:Caf1) (Table S3). Hence, the open UBS conformation in the Caf1-bound chaperone is predesigned for optimal binding to Caf1A.

To confirm the role of the proline lock in regulating the affinity of Caf1M to Caf1A, it would be logical to break the lock in Caf1M and demonstrate Caf1M-Caf1A binding. However, because the residues comprising the lock also participate directly in Caf1M-Caf1A binding, simple substitution mutagenesis of the lock residues would not provide a clear answer. Hence, we chose a different approach. The proline lock residues mark the beginning of the subunit-binding $F_1G_1$ hairpin loop. We hypothesized that shortening this loop may generate a stretching force pulling on the loop, including the proline lock, thus forcing it to disengage and allow the UBS to open. We created a series of Caf1M mutants with shorter $F_1G_1$ loops (Table 2; Table S1). As we predicted, the affinity of free Caf1M to $Caf1A_N$ gradually increased with the length of deletion (Table 2). Caf1M 106-129 bound to $Caf1A_N$ with a dissociation constant of 9.8 ± 1.0 μM and efficiently inhibited $Caf1A_N$-(Caf1M:Caf1) binding (Figure S2).

In conclusion, our structural-biochemical study suggests an allosteric mechanism, in which Pro103[m] and Pro104[m] act in concert as a "proline lock" that prevents or allows usher binding, depending on whether the subunit is bound or not (Figure 6; Movie S1). In free Caf1M, the lock keeps the UBS closed, preventing Caf1M from binding to Caf1A. Caf1 binding unlocks the proline lock and opens the UBS, allowing the Caf1M:Caf1 complex to target and bind to Caf1A.

## Communication between the Caf1 and Caf1A Binding Sites in Caf1M

How does Caf1 binding switch the UBS conformation from closed to open? As Caf1 does not form direct interactions with the UBS residues, we considered possible mechanisms for communication between the Caf1 and Caf1A binding sites in Caf1M.

Upon Caf1M:Caf1 complex formation, the 11-residue-long C-terminal part of the $F_1G_1$ loop (residues 124–134) forms a donor beta strand that binds in the acceptor cleft of the subunit to compensate for the lacking G β strand (Figures 4A and 6A). As the extended structure of the donor strand forms, the $F_1G_1$ loop is shortened, considerably reducing its conformational freedom. We hypothesized that this might result in a stretching force pulling on the loop that might be sufficient to open the proline lock, as we observed for artificially short $F_1G_1$ loops. To investigate this hypothesis, we created a series of Caf1M mutants with longer $F_1G_1$ loops (Table 2; Table S1). We expected that the

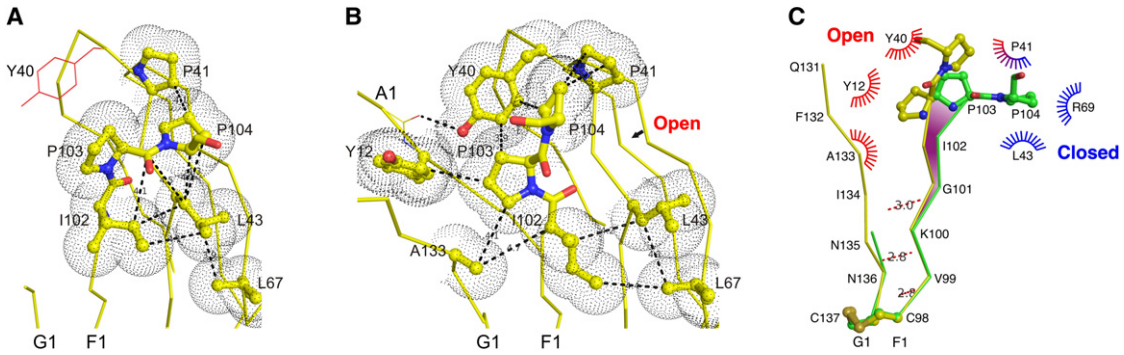


**Figure 5. Caf1 Binding Opens the Pro-Pro Lock by Generating an Alternative Hydrophobic Pro-Pro Pocket**

(A) The binding site for Pro104$^m$ in Caf1-free Caf1M (residues Pro41$^m$, Leu43$^m$, and Ile102$^m$). Residues involved in the binding and UBS are shown as balls and sticks painted by atom colors (yellow – carbon; red – oxygen; blue – nitrogen). Atomic radii are indicated with mesh. Distances between interacting atoms are indicated in Å. The main chain is shown as ribbon painted in yellow color.

(B) The binding sites for Pro103$^m$ and Pro104$^m$ in Caf1-bound Caf1M (residues Tyr12$^m$, Tyr40$^m$, Pro41$^m$, and Ala133$^m$).

(C) Schematic diagram of the open (yellow) and closed (green) lock. The shaded area indicates the movement of the $F_1$ strand caused by its twist upon complex formation. Dashed lines indicate hydrogen bonds that form between the $F_1$ and $G_1$ strands in the complex. The disulfide bond stabilizing the $F_1G_1$ hairpin is shown.

See also Figure S4.

loop extension would reduce any stretching force, leaving the UBS in the closed conformation. Such mutant Caf1M:Caf1 complexes should not bind to Caf1A. Indeed, we found that all mutants with the $F_1G_1$ loop extended by at least two residues at two different sites (Ala114$^m$ and Asp123$^m$) bind about two times weaker to Caf1A$_N$ than the wild-type complex. However, our crystal structure of the Caf1M:Caf1 complex carrying the insertion KDKDTN at Ala114$^m$ reveals an open UBS (Figure S4A). Hence, at least in Caf1M, with its exceptionally long $F_1G_1$ loop, a stretching force alone is not sufficient to switch the UBS from the closed to the open conformation.

Caf1 binding changes the local environment of the lock (Figure 5B). In the Caf1M:Caf1 complex, Tyr12$^m$ and Ala133$^m$ from the $A_1$ and $G_1$ donor strands, respectively, form van der Waals interactions with Pro103$^m$. In addition, the side chain of Tyr40$^m$, which in Caf1M:Caf1 is linked to the main chain of the $A_1$ donor strand via a hydroxyl-amide hydrogen bond, forms extensive interactions with both Pro103$^m$ and Pro104$^m$. These interactions are absent in free Caf1M, because the concerned Caf1-binding segments are unstructured.

To examine whether these interactions are sufficient to maintain an open UBS, we replaced Tyr12$^m$ by Gly and Tyr40$^m$ by Ala residues and analyzed the effect of these mutations on the affinity of the Caf1M:Caf1 complex to Caf1A$_N$ (Table 2) and efficiency of F1 capsule assembly (Figure 3). Both single mutations decreased the affinity, in particular Tyr40$^m$Ala, which also clearly inhibited surface assembly. Combined, the mutations led to a dramatic effect: both Caf1A$_N$-(Caf1M:Caf1) binding and assembly were practically abolished.

We hypothesized that mutations that disrupt the Pro103$^m$ Pro104$^m$ binding pocket Tyr12$^m$-Tyr40$^m$-Ala133$^m$ would favor the collapsed proline lock conformation and keep the UBS closed. Indeed, our crystal structure of the Caf1M:Caf1 complex carrying the Tyr40$^m$Ala mutation revealed the closed conformation (Figure S4A), demonstrating that the local environment around the proline lock in the preassembly complex maintains its extended conformation and is critical for keeping the UBS open. Tyr12$^m$ and Tyr40$^m$ occupy highly conserved positions in multiple sequence alignments of FGL chaperones, suggesting that they all employ a similar allosteric communication mechanism.

In the absence of pocket Tyr12$^m$-Tyr40$^m$-Ala133$^m$ (formed only after Caf1 binding), Pro104$^m$ can instead insert into a hydrophobic pocket formed by Pro41$^m$, Leu43$^m$, and Ile102$^m$, closing the UBS (Figure 5A). A strong tendency to attain this conformation is suggested by our molecular dynamics (MD) simulations (Figure S4B). The Caf1M model with the open UBS (taken from the crystal structure of the Caf1M:Caf1 complex) was subjected to MD simulations in an aqueous environment. The UBS became substantially closed within a 20–25 ps time interval, which is reflected in the change of the distance between Cα atoms of Pro104$^m$ and Leu43$^m$ from 8.3 to 6.5 Å. MD simulations with the Leu43Ala mutant of Caf1M showed a somewhat intermediate conformation between closed and open UBS with a 7.4 Å distance between Cα atoms of Pro104$^m$ and Ala43$^m$, suggesting that the switch is driven not only by the hydrophobic effect. The twist in the $F_1$ strand may also facilitate opening the UBS, as it contributes to rotation of the proline lock residues (Figure 5C).

## Control of Subunit Trafficking in Other Chaperone/Usher Systems

To investigate if binding of preassembly complexes to the usher may be controlled through a similar allosteric proline lock mechanism in other chaperone/usher systems, we examined available structures of subunit-free and bound chaperones (Table S3).

Currently, structures for two FGL (Caf1M and SafB) and four FGS chaperones (FimC, PapD, FaeE, and SfaE) have been deposited in the protein data bank (PDB). With exception for SfaE, all these chaperones have been cocrystallized with corresponding organelle subunits, providing a wealth of structural information on the subunit-bound chaperone conformation. Superposition of UBSs in the subunit-bound structures together

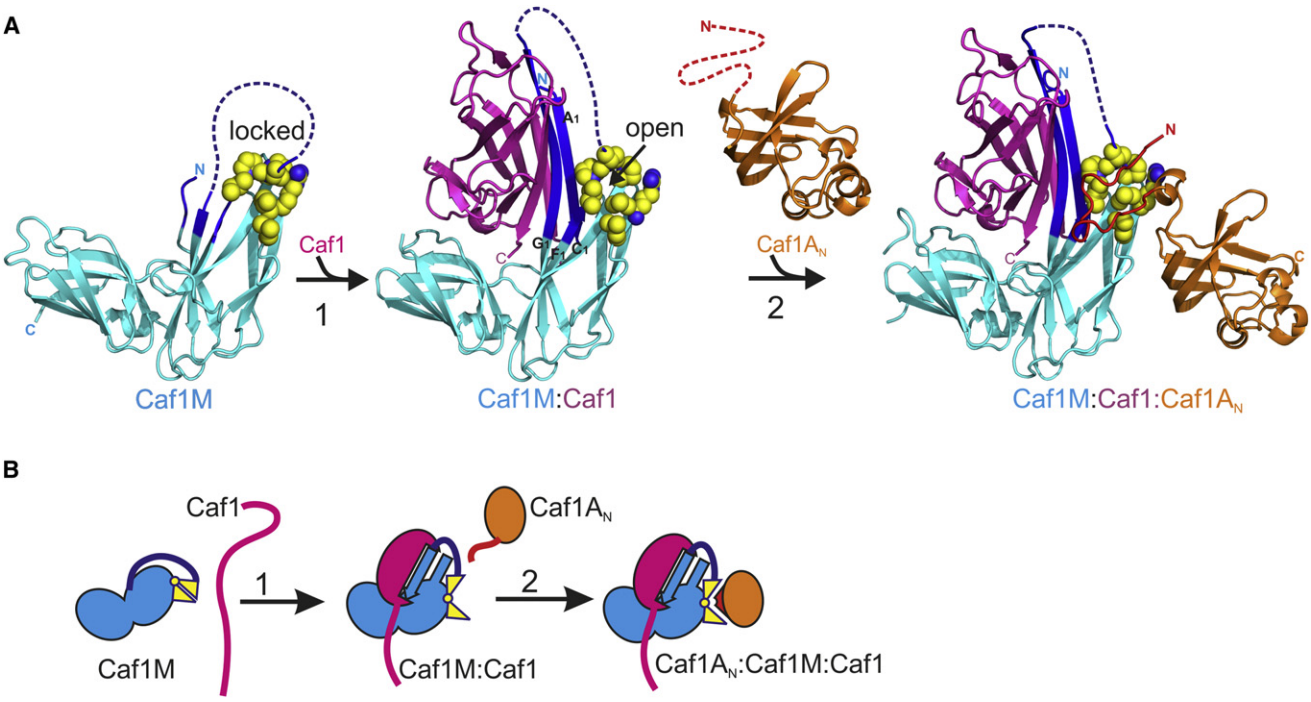


**Figure 6. Caf1-Induced Changes in Caf1M Enable Caf1M Binding to Caf1A**

(A) Crystal structures of the Caf1M monomer (Caf1M-Δ2-12, -Δ113-129), preassembly complex Caf1M:Caf1, Caf1A$_N$ domain of Caf1A, and Caf1A$_N$:Caf1M:Caf1 complex (cartoon diagrams), illustrating the chaperone-subunit binding (1) and usher targeting (2) steps of the assembly process. The regions in the N-terminal sequence and $F_1G_1$ hairpin of Caf1M that become structured upon subunit binding are shown in blue; the rest of Caf1M is in cyan. Caf1 is shown in magenta. Caf1A$_N$ is shown in orange, except the N-terminal segment, which becomes ordered on binding of chaperone: subunit complex and is shown in red. Side chains of residues Pro41$^m$, Leu43$^m$, Leu67$^m$, Ile102$^m$, Pro103$^m$, Pro104$^m$, and aliphatic atoms of Arg69$^m$ comprising the usher binding surface (UBS) are shown as spheres, and Pro103$^m$ is labeled. The disordered part of the $F_1G_1$ loop (not observed in crystal structures) is indicated with dashed lines. See also Movie S1.

(B) Schematic representation of structures shown in (A).

with that of Caf1M in Caf1M:Caf1 demonstrates that, regardless of the type of the chaperone, all of them have an open UBS (for superposition of prototypical FGL and FGS chaperones, see Figure 7A). The distance between Cα atoms in residues corresponding to Pro104 and Leu43 of Caf1M in subunit-bound FimC, PapD, and SafB is universally long (7.7–8.1 Å) and is practically independent of the type of the bound subunit. Only in the FaeE:FaeF complex, this distance is slightly shorter (7.3 Å). This is probably due to the absence of a bulky side chain at the usher-binding position (e.g., Leu43 in Caf1M and Gly32 in FaeE).

As is the case for the Caf system, the structure of the Fim system UBS is almost identical in the free chaperone:subunit preassembly complex and in the usher-bound complex. This confirms that the open conformation of the UBS, which is present in all chaperone:subunit complexes, is optimal for usher binding.

The subunit-free chaperone conformation is best studied for FimC and PapD (Table S3). For PapD, several crystal structures were determined (Holmgren and Bränden, 1989; Hung et al., 1999; Pinkner et al., 2006), while FimC was solved by nuclear magnetic resonance (NMR) (Pellecchia et al., 1998). Although Caf1M and PapD or FimC belong to different chaperone families, the structures of their UBSs can be nicely superimposed (Figure 7A), which clearly demonstrates that, as for Caf1M, subunit-free FimC and PapD have a closed UBS. This is reflected in a 2 to 3 Å shorter distance between Cα atoms of Leu32-Ser92 and Leu32-Pro95 in FimC and PapD, respectively (Table S3). Whereas part of the $F_1G_1$ strand remains invisible in all of the crystal structures, the entire $F_1G_1$ loop is seen in the NMR structure of FimC. The loop region is highly flexible and is represented by quite different NMR traces. Nevertheless, in the majority of the representative NMR traces, the loop is positioned above the closed UBS, thus creating an additional steric obstacle for chaperone-usher binding.

Unfortunately, not all crystal structures of subunit-free chaperones can provide information about the conformation of the UBS. The complication arises from the fact that chaperones tend to form "self-capping" dimers or, in the case of wild-type Caf1M, tetramers, in which the subunit binding motifs are engaged in oligomerization. This self-capping mechanism mimics chaperone-subunit interactions and hence may directly affect the structure of the UBS. Self-capping is observed in crystal structures of the FaeE and SfaE chaperones, causing an unusually open UBS in these structures (Table S3).

Classical FGS CU machineries systems typically assemble complex structures consisting of several different subunits. In the Pap system, the order of assembly of subunits in the fiber apparently correlates with the affinity of the corresponding chaperone-subunit complexes to the usher (Dodson et al., 1993), and in both Pap and Fim systems, the chaperone:adhesin subunit

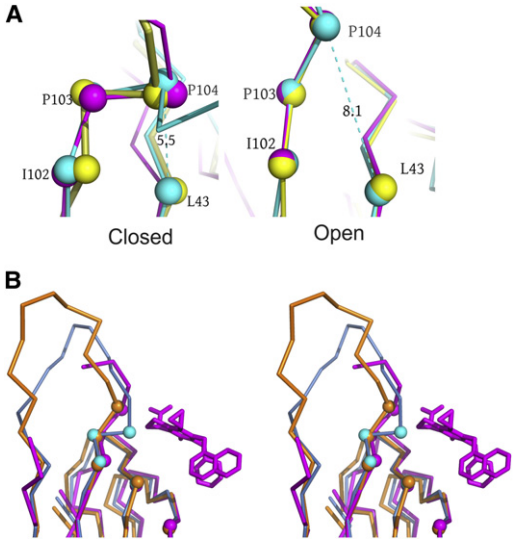


**Figure 7. Allosteric Regulation of Chaperone Assisted Transport in FGS Chaperone/Usher Systems**

(A) Closed and open UBS in two prototypical FGS chaperones, PapD and FimC (in comparison with Caf1M). Crystal structures of subunit-free (left) and subunit-bound (right) Caf1M (magenta), PapD (yellow), and FimC (cyan) were superimposed by distance minimization between Cα atoms of the key usher-binding residues.

(B) Pilicide binding causes opening of the UBS in PapD. Superposition of subunit-free PapD (blue), subunit-free PapD bound to pilicide (magenta), and the PapK subunit bound PapD (orange). Cα atoms of key usher-binding residues of the chaperone are shown as spheres.

See Table S3 for the details.

complexes bind to the usher tighter and faster than structural subunits (Nishiyama and Glockshuber, 2010; Saulino et al., 1998). How does the usher detect the type of subunit loaded to the chaperone in these systems? Nashiyama et al. (2005) suggested that the usher discriminately recognizes subunits by establishing direct binding contacts with them. Indeed, the interactive area between $FimD_N$ and FimH is significantly larger than that between $FimD_N$ and FimF in the corresponding usher domain:chaperone:subunit complexes (Eidam et al., 2008; Nishiyama et al., 2005), which positively correlates with the affinity between the usher and corresponding preassembly complexes (Nishiyama et al., 2003). However, in view of the very limited usher-subunit binding area in the FimD:FimC:FimF complex (Eidam et al., 2008), it is difficult to explain why $FimD_N$ binds tighter to FimC:FimF than to FimC:FimA (Nishiyama et al., 2003). Our discovery of regulation of the affinity of the chaperone to the usher by subunit binding suggests an alternative mechanism. Different subunits might differently affect the UBS conformation, resulting in different affinities of the same chaperone to the usher. Interestingly, the conformation of the $A_1A_2$ loop in subunits in chaperone:subunit complexes that bind poorly to the usher (PapA, PapH, and FimA) is different from that in subunits in chaperone:subunit complexes that bind tightly to the usher (e.g., PapG, FimH, and FimF) (Choudhury et al., 1999; Crespo et al., 2012; Verger et al., 2006, 2007; Volkan et al., 2012). The $A_1A_2$ loop directly interacts with the lock and closely positioned residues of the chaperone, affecting their positions. These conformational changes could potentially be involved in modulating the affinity of the complexes to the usher.

## Conclusions

In this study, we discovered that trafficking through the Caf CU pathway is allosterically controlled. We show that the Caf1M chaperone contains a structural lock that blocks binding of the free chaperone to the Caf1A usher and that Caf1 binding to Caf1M disengages the lock by allosterically inducing conformational changes in the $Caf1A_N$ binding surface of Caf1M (UBS). This dramatically increases the affinity of Caf1M for $Caf1A_N$ and thus enables selective binding of Caf1-loaded Caf1M to $Caf1A_N$. The generality of this mechanism is strongly supported by analysis of available structures of subunit-free chaperones and chaperone:subunit and usher:chaperone:subunit complexes from other systems, as well as by the high conservation of involved residues.

The switch between a closed UBS in free chaperone and an open UBS capable of binding to the usher in a subunit-loaded chaperone involves a conformational change affecting the positioning of two highly conserved proline residues at the beginning of the $F_1G_1$ loop. In contrast to the "proline switches" found in a number of proteins, e.g., (OuYang et al., 2008; Sarkar et al., 2011; Vogel et al., 2006), the switch between open and closed UBS conformations does not involve Pro cis-trans isomerization. Instead, subunit binding leads to formation of an extended beta strand interaction between the $G_1$ (donor) and $F_1$ strands that twists the $F_1$ strand and rotates the proline lock to the open position, where it is stabilized by a pocket created only after subunit binding.

The subunit-induced changes in the UBS may control not only usher targeting by the chaperone:subunit complexes, but also other steps of subunit trafficking. Thus, the step of subunit incorporation into the growing fiber almost certainly relies on this mechanism. At this step, the newly incoming chaperone:subunit complex replaces the fiber-capping chaperone, allowing chaperone recycling. According to our results, this should be accompanied by the closure of the UBS of the released chaperone. As a consequence of this conformational change, the chaperone would lose its affinity to the UND, preventing free chaperone from inhibiting the capture step by rebinding to the UND. Since the UND and UCD2 domains bind to overlapping sites in the chaperone, rebinding to the UCD might also be prevented. This model is consistent with the levels of energy involved in the process. The Caf1M-Caf1 binding is at least 10 times tighter (Yu et al., 2012) than $Caf1A_N$-(Caf1M:Caf1) binding (Table 2). Hence, Caf1M-Caf1 association could generate sufficient energy to open the UBS and thus allow $Caf1A_N$-(Caf1M:Caf1) binding.

The assembly of type 1 and P pili can be blocked by a specially designed organic molecule called pilicide, which has been shown to specifically inhibit binding of the chaperone:subunit complex to the usher (Pinkner et al., 2006). The crystal structure of a PapD:pilicin complex shows that pilicide binds to the UBS. One of the major contacts is mediated by the pyridone ring of pilicide, which inserts into the subpocket between Leu32, Ile93, and Pro95. Not surprisingly, this binding causes opening of the UBS, increasing the Leu32-Pro95 Cα distance by 3 Å (Figure 7B; Table S3). The better fit of the pilicide to the open UBS explains why it has higher affinity to the chaperone:subunit complex than to the subunit-free chaperone (Pinkner et al., 2006). Hence, to target

subunit-free chaperones, the inhibitor needs to bind and stabilize the closed conformation of the UBS. This alternative approach may help to design inhibitors with binding affinities higher than that of pilicide, which is active only at high (mM) concentrations. Such inhibitors could be used as a starting point for development of novel drugs targeting Gram-negative pathogens.

Many biological pathways are controlled through allosteric mechanisms. Most known cases involve metabolic or signaling pathways, where allosteric control is exerted though key enzymes or signal receptors. Our results extend the concept of allosteric control by providing the example of its use to control trafficking through a protein assembly and secretion pathway assisted by a chaperone.

## EXPERIMENTAL PROCEDURES

### Protein Expression, Purification, and Crystallization

All proteins were expressed in the periplasm of BL21 Star (DE3) cells carrying expression plasmids (see plasmid construction and mutagenesis in Supplemental Experimental Procedures) and extracted by osmotic shock, as described before (Chapman et al., 1999).

Caf1$A_N$ and its mutants were precipitated from the periplasmic fraction by ammonium sulfate to 60% saturation on ice for over 1 hr. Precipitated protein was collected by 20 min centrifugation at 20,000 × *g* and dissolved in water. After dialysis against 5 mM Bis-Tris propane buffer, pH 6.5, protein was loaded onto a MonoQ 10/100 column (GE Healthcare) equilibrated with 20 mM Bis-Tris propane buffer, pH 6.5 (AEX buffer). Proteins bound to the column were eluted using a linear gradient of 0–150 mM NaCl. Caf1M and its mutants were precipitated from the periplasmic fraction as above, dissolved in 20 mM HEPES, pH 7.5, dialyzed against the same buffer, and purified by cation exchange in 50 mM HEPES, pH 7.5, on MonoS 10/100 or HR 5 columns (GE Healthcare) using a linear gradient of 0–200 mM NaCl. The binary complex Caf1M:Caf1-$His_6$ was expressed in *E. coli* and purified as previously described (Zavialov et al., 2003b). The tertiary complex Caf1$A_N$:Caf1M:Caf1 was formed in vitro by mixing Caf1$A_N$ with ~1.5 time molar excess of the purified binary complex Caf1M:Caf1. The latter was obtained by enzymatic cleavage of the N-terminal $His_6$ tag from the Caf1M:Caf1-$His_6$ complex using the TAGzyme protease (QIAGEN). After incubation overnight at 37°C, the tertiary complex was purified using anion-exchange chromatography on a MonoQ 10/100 column in the AEX buffer using a linear gradient of 20–175 mM NaCl. To obtain highest purity samples, proteins were subjected to gel filtration on a Superdex-75 or 200 16/60 HiLoad column (GE Healthcare) equilibrated with 50 mM HEPES, pH 7.4, containing 150 mM NaCl.

Proteins were crystallized by the hanging or sitting drop vapor-diffusion method at 293 K, except for the Caf1$A_N$:Caf1M:Caf1 complex, which was crystallized at 279 K. Caf1$A_N$, Caf1$A_N$:Caf1M:Caf1, and Caf1M-Δ2-12, -Δ113-129 formed crystals in drops containing 20% PEG 3350, 0.2 M ammonium nitrate, pH 6.3; 15% PEG 3350, 0.1 M Na-cacodylate, pH 6.4; and 40% PEG 600 and 0.1 M citrate, pH 5.5; respectively. Crystallization of Caf1M:Caf1 complexes carrying mutations in Caf1M (Y40A and A114-insKDKDTN) were performed as described in Zavialov et al. (2003a).

### Structure Determination and Refinement

X-ray diffraction data were collected at the ESRF beamlines ID14-1, ID 14-4, and ID 29 at 100 K. The structure of the Caf1$A_N$:Caf1M:Caf1 complex was solved by molecular replacement using our crystal structure of the binary Caf1M:Caf1 complex (PDB code 1P5V). The structure of the Caf1$A_N$ domain was built manually in the electron density. The crystal structure of the N-terminal domain from the FimD usher (PDB code 1ZE3) was used as a reference in the initial building cycles. The structure of free Caf1$A_N$ was solved by molecular replacement. The search model included residues 30–120 of the Caf1$A_N$ model from the Caf1$A_N$:Caf1M:Caf1 complex structure. Structures of Caf1M tetramer and the Caf1M:Caf1 complex (PDB accession numbers 2OS7 and 1P5V, respectively) were remodeled to place missing Pro104 and Lys105 into the available electron density. Structures of Caf1M:Caf1 complexes carrying mutations and Caf1M-Δ2-12, -Δ113-129 were solved by molecular replacement using structures of the wild-type complex and a monomer from the Caf1M tetramer structure as search models, respectively. PHASER (McCoy, 2007), REFMAC (Murshudov et al., 1997), and O (Jones et al., 1991) programs were used to perform molecular replacement, structure refinement, and model building, respectively. Data collection and refinement statistics are presented in Table 1. Figure S5 illustrates electron density in the proline lock region.

### Plasmon Resonance Binding Assay

A Biacore X100 system (GE Healthcare) was used for all biosensor experiments. Caf1$A_N$ (approximately 800 resonance units (RU)) was immobilized on flow cell 2 of a CM5 sensor chip by amine coupling using an Amine Coupling Kit (GE Healthcare). To record the association and dissociation curves, samples of Caf1M:Caf1 or Caf1M at varying concentrations were injected into flow cell 2 of the chip for 1 min followed by flushing of the cell with running buffer (10 mM HEPES, pH 7.4, 150 mM NaCl, 3 mM EDTA, 0.005% Tween 20) for 3 min at a flow rate of 10 μl/min. Identical samples were injected over a control flow cell to determine nonspecific binding, which was subtracted from the experimental curves. After each data acquisition cycle, the chip was fully regenerated by an additional 1 min buffer flow.

### Surface Immunofluorescence Assay

DH5α cells transformed with the p12R plasmid carrying wild-type or mutated *Caf* operon (see Supplemental Experimental Procedures) were grown to optical density (OD) 1 at 600 nm. 0.1 $OD_{600nm}$ ml cells were incubated successively with rabbit anti-Caf1SC antibody and goat antirabbit IgG fluorescein conjugate (Sigma) diluted 500 and 50 times with phosphate saline buffer, respectively, followed by measuring fluorescence on a Varian CARY Eclipse fluorescent spectrophotometer (Varian). *E. coli* DH5a/pUC19 was used as a background control.

## ACCESSION NUMBERS

Coordinates of the protein atoms, together with structure factors, for Caf1$A_N$, Caf1$A_N$:Caf1M:Caf1, Caf1M-Δ2-12,-Δ113-129, Caf1M-Y40A:Caf1, and Caf1M-A114-insKDKDTN:Caf1 have been deposited in the Protein Data Bank under accession numbers 4B0E, 4B0M, 4AY0, 4AYF, and 4AZ8, respectively.

## SUPPLEMENTAL INFORMATION

Supplemental Information includes three tables, five figures, Supplemental Experimental Procedures, and one movie and can be found with this article online at http://dx.doi.org/10.1016/j.str.2012.08.016.

## ACKNOWLEDGMENTS

This work was supported by Grants SRC-6212005-5360, FORMAS-221-2007-1057, FA-136333, and FA-140959 to A.V.Z.; VR-2009-5334 to S.D.K.; and BBSRC C514782 and –B-08356 to S.M. We would like to thank the staff at the ESRF (Grenoble, France) for their kind help during data collection and Snezana Vasiljevic for confocal images and her contribution to early stages of the Caf1$A_N$ study.

Received: April 27, 2012
Revised: August 1, 2012
Accepted: August 13, 2012
Published online: September 13, 2012

## REFERENCES

Chapman, D.A.G., Zavialov, A.V., Chernovskaya, T.V., Karlyshev, A.V., Zav'yalova, G.A., Vasiliev, A.M., Dudich, I.V., Abramov, V.M., Zav'yalov, V.P., and MacIntyre, S. (1999). Structural and functional significance of the FGL sequence of the periplasmic chaperone Caf1M of *Yersinia pestis*. J. Bacteriol. *181*, 2422–2429.

Choudhury, D., Thompson, A., Stojanoff, V., Langermann, S., Pinkner, J., Hultgren, S.J., and Knight, S.D. (1999). X-ray structure of the FimC-FimH

chaperone-adhesin complex from uropathogenic *Escherichia coli*. Science *285*, 1061–1066.

Crespo, M.D., Puorger, C., Scharer, M.A., Eidam, O., Grutter, M.G., Capitani, G., and Glockshuber, R. (2012). Quality control of disulfide bond formation in pilus subunits by the chaperone FimC. Nat Chem Biol. Published online July 1, 2012. http://dx.doi.org/10.1038/nchembio.1019.

Dodson, K.W., Jacob-Dubuisson, F., Striker, R.T., and Hultgren, S.J. (1993). Outer-membrane PapC molecular usher discriminately recognizes periplasmic chaperone-pilus subunit complexes. Proc. Natl. Acad. Sci. USA *90*, 3670–3674.

Dubnovitsky, A.P., Duck, Z., Kersley, J.E., Härd, T., MacIntyre, S., and Knight, S.D. (2010). Conserved hydrophobic clusters on the surface of the Caf1A usher C-terminal domain are important for F1 antigen assembly. J. Mol. Biol. *403*, 243–259.

Eidam, O., Dworkowski, F.S., Glockshuber, R., Grütter, M.G., and Capitani, G. (2008). Crystal structure of the ternary FimC-FimF(t)-FimD(N) complex indicates conserved pilus chaperone-subunit complex recognition by the usher FimD. FEBS Lett. *582*, 651–655.

Holmgren, A., and Bränden, C.-I. (1989). Crystal structure of chaperone protein PapD reveals an immunoglobulin fold. Nature *342*, 248–251.

Hung, D.L., Knight, S.D., Woods, R.M., Pinkner, J.S., and Hultgren, S.J. (1996). Molecular basis of two subfamilies of immunoglobulin-like chaperones. EMBO J. *15*, 3792–3805.

Hung, D.L., Pinkner, J.S., Knight, S.D., and Hultgren, S.J. (1999). Structural basis of chaperone self-capping in P pilus biogenesis. Proc. Natl. Acad. Sci. USA *96*, 8178–8183.

Jones, T.A., Zou, J.Y., Cowan, S.W., and Kjeldgaard, M. (1991). Improved methods for building protein models in electron density maps and the location of errors in these models. Acta Crystallogr. A *47*, 110–119.

MacIntyre, S., Zyrianova, I.M., Chernovskaya, T.V., Leonard, M., Rudenko, E.G., Zav'Yalov, V.P., and Chapman, D.A.G. (2001). An extended hydrophobic interactive surface of *Yersinia pestis* Caf1M chaperone is essential for subunit binding and F1 capsule assembly. Mol. Microbiol. *39*, 12–25.

McCoy, A.J. (2007). Solving structures of protein complexes by molecular replacement with Phaser. Acta Crystallogr. D Biol. Crystallogr. *63*, 32–41.

Murshudov, G.N., Vagin, A.A., and Dodson, E.J. (1997). Refinement of macromolecular structures by the maximum-likelihood method. Acta Crystallogr. D Biol. Crystallogr. *53*, 240–255.

Nishiyama, M., and Glockshuber, R. (2010). The outer membrane usher guarantees the formation of functional pili by selectively catalyzing donor-strand exchange between subunits that are adjacent in the mature pilus. J. Mol. Biol. *396*, 1–8.

Nishiyama, M., Vetsch, M., Puorger, C., Jelesarov, I., and Glockshuber, R. (2003). Identification and characterization of the chaperone-subunit complex-binding domain from the type 1 pilus assembly platform FimD. J. Mol. Biol. *330*, 513–525.

Nishiyama, M., Horst, R., Eidam, O., Herrmann, T., Ignatov, O., Vetsch, M., Bettendorff, P., Jelesarov, I., Grütter, M.G., Wüthrich, K., et al. (2005). Structural basis of chaperone-subunit complex recognition by the type 1 pilus assembly platform FimD. EMBO J. *24*, 2075–2086.

OuYang, B., Pochapsky, S.S., Dang, M., and Pochapsky, T.C. (2008). A functional proline switch in cytochrome P450cam. Structure *16*, 916–923.

Pellecchia, M., Güntert, P., Glockshuber, R., and Wüthrich, K. (1998). NMR solution structure of the periplasmic chaperone FimC. Nat. Struct. Biol. *5*, 885–890.

Phan, G., Remaut, H., Wang, T., Allen, W.J., Pirker, K.F., Lebedev, A., Henderson, N.S., Geibel, S., Volkan, E., Yan, J., et al. (2011). Crystal structure of the FimD usher bound to its cognate FimC-FimH substrate. Nature *474*, 49–53.

Pinkner, J.S., Remaut, H., Buelens, F., Miller, E., Aberg, V., Pemberton, N., Hedenström, M., Larsson, A., Seed, P., Waksman, G., et al. (2006). Rationally designed small compounds inhibit pilus biogenesis in uropathogenic bacteria. Proc. Natl. Acad. Sci. USA *103*, 17897–17902.

Remaut, H., Rose, R.J., Hannan, T.J., Hultgren, S.J., Radford, S.E., Ashcroft, A.E., and Waksman, G. (2006). Donor-strand exchange in chaperone-assisted pilus assembly proceeds through a concerted beta strand displacement mechanism. Mol. Cell *22*, 831–842.

Remaut, H., Tang, C., Henderson, N.S., Pinkner, J.S., Wang, T., Hultgren, S.J., Thanassi, D.G., Waksman, G., and Li, H. (2008). Fiber formation across the bacterial outer membrane by the chaperone/usher pathway. Cell *133*, 640–652.

Sarkar, P., Saleh, T., Tzeng, S.R., Birge, R.B., and Kalodimos, C.G. (2011). Structural basis for regulation of the Crk signaling protein by a proline switch. Nat. Chem. Biol. *7*, 51–57.

Sauer, F.G., Fütterer, K., Pinkner, J.S., Dodson, K.W., Hultgren, S.J., and Waksman, G. (1999). Structural basis of chaperone function and pilus biogenesis. Science *285*, 1058–1061.

Sauer, F.G., Pinkner, J.S., Waksman, G., and Hultgren, S.J. (2002). Chaperone priming of pilus subunits facilitates a topological transition that drives fiber formation. Cell *111*, 543–551.

Saulino, E.T., Thanassi, D.G., Pinkner, J.S., and Hultgren, S.J. (1998). Ramifications of kinetic partitioning on usher-mediated pilus biogenesis. EMBO J. *17*, 2177–2185.

Verger, D., Miller, E., Remaut, H., Waksman, G., and Hultgren, S. (2006). Molecular mechanism of P pilus termination in uropathogenic Escherichia coli. EMBO Rep. *7*, 1228–1232.

Verger, D., Bullitt, E., Hultgren, S.J., and Waksman, G. (2007). Crystal structure of the P pilus rod subunit PapA. PLoS Pathog. *3*, e73.

Vogel, M., Bukau, B., and Mayer, M.P. (2006). Allosteric regulation of Hsp70 chaperones by a proline switch. Mol. Cell *21*, 359–367.

Volkan, E., Ford, B.A., Pinkner, J.S., Dodson, K.W., Henderson, N.S., Thanassi, D.G., Waksman, G., and Hultgren, S.J. (2012). Domain activities of PapC usher reveal the mechanism of action of an Escherichia coli molecular machine. Proc. Natl. Acad. Sci. USA *109*, 9563–9568.

Waksman, G., and Hultgren, S.J. (2009). Structural biology of the chaperone-usher pathway of pilus biogenesis. Nat. Rev. Microbiol. *7*, 765–774.

Yu, X., Visweswaran, G.R., Duck, Z., Marupakula, S., MacIntyre, S., Knight, S.D., and Zavialov, A.V. (2009). Caf1A usher possesses a Caf1 subunit-like domain that is crucial for Caf1 fibre secretion. Biochem. J. *418*, 541–551.

Yu, X.D., Fooks, L.J., Moslehi-Mohebi, E., Tischenko, V.M., Askarieh, G., Knight, S.D., Macintyre, S., and Zavialov, A.V. (2012). Large is fast, small is tight: determinants of speed and affinity in subunit capture by a periplasmic chaperone. J. Mol. Biol. *417*, 294–308.

Zavialov, A.V., and Knight, S.D. (2007). A novel self-capping mechanism controls aggregation of periplasmic chaperone Caf1M. Mol. Microbiol. *64*, 153–164.

Zavialov, A.V., Berglund, J., and Knight, S.D. (2003a). Overexpression, purification, crystallization and preliminary X-ray diffraction analysis of the F1 antigen Caf1M-Caf1 chaperone-subunit pre-assembly complex from Yersinia pestis. Acta Crystallogr. D Biol. Crystallogr. *59*, 359–362.

Zavialov, A.V., Berglund, J., Pudney, A.F., Fooks, L.J., Ibrahim, T.M., MacIntyre, S., and Knight, S.D. (2003b). Structure and biogenesis of the capsular F1 antigen from Yersinia pestis: preserved folding energy drives fiber formation. Cell *113*, 587–596.

Zavialov, A.V., Tischenko, V.M., Fooks, L.J., Brandsdal, B.O., Aqvist, J., Zav'yalov, V.P., Macintyre, S., and Knight, S.D. (2005). Resolving the energy paradox of chaperone/usher-mediated fibre assembly. Biochem. J. *389*, 685–694.

Zavialov, A.V., Zav'yalova, G.A., Korpela, T., and Zav'yalov, V.P. (2007). FGL chaperone-assembled fimbrial polyadhesins: anti-immune armament of Gram-negative bacterial pathogens. FEMS Microbiol. Rev. *31*, 478–514.

Zav'yalov, V.P., Zav'yalova, G.A., Denesyuk, A.I., and Korpela, T. (1995). Modelling of steric structure of a periplasmic molecular chaperone Caf1M of Yersinia pestis, a prototype member of a subfamily with characteristic structural and functional features. FEMS Immunol. Med. Microbiol. *11*, 19–24.

Zav'yalov, V., Zavialov, A., Zav'yalova, G., and Korpela, T. (2010). Adhesive organelles of Gram-negative pathogens assembled with the classical chaperone/usher machinery: structure and function from a clinical standpoint. FEMS Microbiol. Rev. *34*, 317–378.